Research in Astronomy and Astrophysics, 25:045003 (14pp), 2025 April
https://doi.org/10.1088/1674-4527/adbc36
CSTR: 32081.14.RAA.adbc36


# The 12.2 GHz Methanol Masers in the Milky Way with Statistical Analysis

Shi-Min Song[1,2], Xi Chen[2,3], Jun-Ting Liu[2], You-Xin Wang[4], Kai Yang[5,6], Yan-Kun Zhang[2], and Zhang Zhao[2]
[1] School of Mathematics and Information Science, Guangzhou University, Guangzhou 510006, China
[2] Center for Astrophysics, Guangzhou University, Guangzhou 510006, China; chenxi@gzhu.edu.cn
[3] Shanghai Astronomical Observatory, Chinese Academy of Sciences, Shanghai 200030, China
[4] Max-Planck-Institut für Radioastronomie, Auf dem Hügel 69, D-53121 Bonn, Germany
[5] School of Astronomy and Space Science, Nanjing University, Nanjing 210023, China
[6] Key Laboratory of Modern Astronomy and Astrophysics (Nanjing University), Ministry of Education, Nanjing 210023, China
*Received 2024 October 25; revised 2024 December 30; accepted 2025 January 7; published 2025 April 3*

## Abstract

We present the most comprehensive catalog of 12.2 GHz methanol maser sources within the Milky Way to date, consisting of 457 12.2 GHz methanol masers associated with 1085 6.7 GHz methanol masers, resulting in a detection rate of 42%. Distances to these sources are derived from the Bar and Spiral Structure Legacy Survey project Distance Calculator. Our analysis shows that both 6.7 and 12.2 GHz methanol masers are more likely to be excited near galactocentric distances of 5–6 kpc, with the detection rate of 12.2 GHz methanol masers decreasing as the galactocentric distance increases. There are no significant differences in the detection rates of 12.2 GHz masers across the four spiral arms, which consistently range between 40% and 50%. However, the detection rate of 12.2 GHz methanol masers tends to be higher in the heads of the spiral arms compared to the tails. Analysis of data from the APEX Telescope Large Area Survey of the Galaxy (ATLASGAL) indicates that the luminosity of 6.7 GHz masers peaks at a clump dust temperature of about 30 K, while that of 12.2 GHz masers grows with increasing dust temperature. Clumps associated with 12.2 GHz methanol masers generally have higher dust temperatures, bolometric luminosities, and hydrogen densities than those associated only with 6.7 GHz methanol masers or without either maser. Furthermore, clumps in the H II region stage exhibit a higher detection rate of 12.2 GHz masers compared to those in other stages, as indicated by the evolutionary stages derived from the ATLASGAL survey results.

*Key words:* masers – stars: massive – stars: protostars

## 1. Introduction

Methanol molecules are abundant in interstellar space and exhibit a diverse range of transition lines (e.g., Cragg et al. 2005; Goedhart et al. 2005; Chen et al. 2019). The methanol maser transition lines are widely recognized as important tracers of star formation regions (e.g., Ellingsen 2006; Green et al. 2009; Breen et al. 2013; Chen et al. 2014). Methanol masers are classified into two classes based on their different pumping mechanisms (Batrla et al. 1987; Menten & Melnick 1991): Class I methanol masers are primarily pumped by collisions and are often found at locations distant from the radiation source, possibly associated with shock environments, such as molecular outflows (Menten & Melnick 1991); Class II methanol masers are mainly pumped by infrared radiation and are typically found closer to the radiation source (e.g., UC H II region), providing a sensitive probe of variations in the radiation field of young stars.

The 6.7 ($5_1 \rightarrow 6_0 A^+$) and 12.2 ($2_0 \rightarrow 3_{-1} E$) GHz methanol masers, as the most notable Class II methanol masers, are extensively used as crucial tools in studying high-mass star formation regions (HMSFRs; Batrla et al. 1987; Menten 1991; Szymczak et al. 2012; Breen et al. 2015). In recent years, a significant increase in research on high-mass accretion bursts event has been seen, notably marked by the initial detection of four high-mass star accretion events through Class II methanol maser flares (S255IR-NIRS3, Caratti o Garatti et al. 2017; Liu et al. 2018; Uchiyama et al. 2022; NGC 6334I-MM1, Hunter et al. 2017, 2018; G358.93−0.03-MM1, Chen et al. 2020; G24.33+0.14, Kobak et al. 2023). This highlights the growing significance of investigating Class II methanol masers.

Over the past few decades, significant research has focused on the search for 6.7 GHz methanol masers. More than 1000 IRAS sources have been investigated for 6.7 GHz methanol masers (e.g., MacLeod et al. 1992; van der Walt et al. 1995). The Methanol Multi-Beam (MMB) survey using the Parkes telescope (Caswell et al. 2010, 2011; Green et al. 2010, 2012; Breen et al. 2015) conducted an unbiased search across Galactic longitudes from 186° to 60° and latitudes from −2° to +2°, detecting 972 sources with 6.7 GHz methanol maser emissions. Concurrently, Yang et al. (2017, 2019) surveyed approximately 3400 WISE point sources in the northern sky, identifying about 230 sources with 6.7 GHz masers. From these

efforts, Yang et al. (2019) compiled the most comprehensive catalog of 6.7 GHz methanol masers to date, containing 1085 sources.

Although 6.7 GHz methanol masers are well cataloged, their 12.2 GHz counterparts have not been comprehensively summarized. The model proposed by Cragg et al. (2005) suggests that the excitation of both 6.7 and 12.2 GHz methanol masers requires similar physical environments, indicating that targeting 6.7 GHz methanol masers to locate 12.2 GHz counterparts is a viable method. Numerous studies have utilized 6.7 GHz methanol masers as target sources to detect 12.2 GHz methanol masers. For instance, Caswell et al. (1995) investigated 238 6.7 GHz methanol masers associated with OH masers and identified 12.2 GHz methanol masers in 55% of them; MacLeod et al. (1998) detected 12.2 GHz methanol masers toward 24 IRAS sources; Błaszkiewicz & Kus (2004) found 49 sources with 12.2 GHz methanol masers among 121 6.7 GHz methanol masers; Song et al. (2022) targeted 367 sources with 6.7 GHz methanol masers, discovering 176 instances of 12.2 GHz methanol maser emissions. Among these efforts, the most significant findings emerged from the MMB survey (Breen et al. 2012a, 2012b, 2014, 2016), which identified 438 instances of 12.2 GHz methanol masers from 972 sources exhibiting 6.7 GHz methanol masers.

A significant number of 6.7 GHz methanol masers lack 12.2 GHz counterparts (e.g., Breen et al. 2012a, 2012b, 2014), suggesting that the physical conditions necessary for these transitions are not entirely consistent. The exact reasons for the absence of 12.2 GHz masers remain unclear. Multiple studies indicate a close relationship between the fluxes and luminosities of 6.7 and 12.2 GHz methanol masers (e.g., Green et al. 2009, 2017; Breen et al. 2018), yet these masers do not share identical physical conditions in their host environments (e.g., Breen et al. 2012a, 2012b). The 12.2 GHz masers are more sensitive to variations in temperature and density, leading to more pronounced flux variations compared to 6.7 GHz masers. Investigating sources associated only with 6.7 GHz masers may provide insights into the reasons for the non-detection of 12.2 GHz masers.

This work aims to compile and statistically analyze the 12.2 GHz methanol masers within the Milky Way, further exploring the spatial and physical differences between 6.7 and 12.2 GHz methanol masers. The analysis primarily relies on physical parameters of massive clumps from the APEX Telescope Large Area Survey of the Galaxy (ATLASGAL) and employs the distance calculation model from the Bar and Spiral Structure Legacy (BeSSeL) Survey project.

The ATLASGAL survey, an 870 $\mu$m dust survey of the Galactic plane (e.g., Urquhart et al. 2018, 2022), covers 420 square degrees of the inner Milky Way and has identified approximately 10,000 dense molecular clumps. Physical parameters such as dust temperature, bolometric luminosity, and mass have been provided for about 8000 of these clumps. Notably, around 88% of these clumps exhibit star formation activity. Furthermore, 5007 clumps have been classified into four evolutionary stages-quiescent, protostellar, young stellar objects, and H II regions-facilitating the analysis of the evolutionary stages in which 6.7 and 12.2 GHz methanol masers occur.

The BeSSeL project, a VLBA Key Science initiative, accurately measures distances and proper motions of masers across the Milky Way. By determining the trigonometric parallaxes of approximately 200 maser sources, Reid et al. (2016, 2019) developed a model of the spiral arms and provided a comprehensive depiction of the Milky Way. Utilizing this data has significantly aided systematic studies of HMSFR distributions within the galaxy. This paper employs the Galactic kinematic model from the BeSSeL project to calculate distances for Class II methanol maser sources.

The structure of this paper is organized as follows: Section 2 details the methodology for sample selection and observation of the remaining 12.2 GHz methanol masers. Section 3 provides brief comments on the detected 12.2 GHz maser sources. Discussions of the properties of 12.2 GHz masers, including their distribution within the Milky Way, their physical excitation conditions, and their relationships with 6.7 GHz masers, are covered in Section 4. Finally, the conclusions are summarized in Section 5.

## 2. Sample Selection and Observation

### 2.1. Sample Selection

Song et al. (2022) reported 176 12.2 GHz methanol masers toward 367 6.7 GHz methanol masers using the Shanghai Tianma 65 m Radio Telescope (TMRT). According to the catalog of 6.7 GHz methanol masers compiled by Yang et al. (2019), 117 sources had not been systematically explored for 12.2 GHz methanol maser presence in the MMB survey. Consequently, we observed these 117 sources using the TMRT to develop a comprehensive catalog of 12.2 GHz methanol maser sources in the Milky Way (see Table 1).

### 2.2. Observation

Observations were conducted using the TMRT from 2022 May to 2023 September. The TMRT, a fully steerable 65 m diameter radio telescope, utilized a *Ku*-band receiver covering a frequency range of 12–18 GHz, in conjunction with the Digital Backend System (DIBAS). DIBAS, an FPGA-based spectrometer, was developed based on the Versatile GBT Astronomical Spectrometer (Bussa & VEGAS Development Team 2012). Eight spectral windows were employed to simultaneously observe multiple transitions. Each window had a bandwidth of 23.4375 MHz and 8192 channels, yielding a spectral resolution of approximately 0.06 km s$^{-1}$ at 12 GHz. The methanol transition $2_0$–$3_{-1}$ *E* rest frequency, 12178.593 MHz, was covered by one of

**Table 1**
117 Sample Sources in Targeting 12.2 GHz Methanol Maser

| Name (l, b) (1) | R.A. (hhmmss) (2) | Decl. (ddmmss) (3) | rms (Jy) (4) |
|---|---|---|---|
| G0.39−0.03 | 17 46 41.120 | −28 37 05.50 | 0.172 |
| G0.53+0.18 | 17 46 09.800 | −28 23 29.00 | 0.181 |
| G10.09+0.71 | 18 05 18.180 | −19 51 14.50 | 0.159 |
| G10.62−0.29 | 18 10 09.900 | −19 53 22.00 | 0.243 |
| G12.79−0.19 | 18 14 11.100 | −17 55 57.00 | 0.293 |
| G14.33−0.64 | 18 18 53.800 | −16 47 46.60 | 0.163 |
| G23.80+0.40 | 18 33 13.000 | −07 55 41.00 | 0.208 |
| … | … | … | … |

**Note.** Column (1) lists the names of the sources, identified by Galactic longitude and latitude. Columns (2) and (3) display the coordinates of the 6.7 GHz methanol maser sources as compiled in Yang et al. (2019). Column (4) is the 12.2 GHz rms limit obtained for our observations. (The full table is available at https://www.scidb.cn/en/s/BjaUFz).

these windows. System temperatures ranged from 40 to 50 K. The TMRT's aperture efficiency of approximately 55% provided a sensitivity of 1.6 Jy $K^{-1}$. At 12.2 GHz, the beam size was approximately 2′ (HPBW), with flux density uncertainties for detected sources below 10%.

Position-switching mode was employed during our observations. Each source underwent two ON–OFF cycles, with each ON and OFF position lasting a minimum of 2 minutes. The OFF position was offset by (0.°0, −0.°4) in R.A. and decl. from the ON position of the targeted source.

Data processing utilized the GILDAS/CLASS[7] package. For each source, the linear baseline of the spectrum was fitted and subtracted, resulting in a typical rms noise of approximately 0.17 Jy per channel.

## 3. Results

After observing 117 sources, we successfully detected four previously discovered (Błaszkiewicz & Kus 2004; Durjasz et al. 2021) 12.2 GHz methanol masers. The spectra are shown in Figure 1, and Table 2 provides details of these four sources.

Durjasz et al. (2021) investigated 36 sources for 12.2 GHz methanol masers near 6.7 GHz methanol masers. Building on these findings and the MMB 12.2 GHz methanol maser survey (Breen et al. 2012a, 2012b, 2014, 2016), we compiled the most comprehensive catalog of 12.2 GHz methanol masers in the Milky Way to date, listing 457 sources (see Table 3). Notably, all these 12.2 GHz methanol masers were detected among the known 6.7 GHz methanol masers, as included in the sample of 1085 6.7 GHz methanol masers documented by Yang et al. (2019).

[7] http://www.iram.fr/IRAMFR/GILDAS; see Pestalozzi et al. (2005) for more detailed information.

### 3.1. The Four Detected 12.2 GHz Masers

We present detailed information about the properties of the four detected 12.2 GHz methanol masers, with specific emphasis on G109.871+2.114, which displayed significant flux density variations. Below are comments for each source:

*G79.736+0.991*. This source has been observed across multiple epochs for both the 6.7 and 12.2 GHz methanol masers. The peak flux densities of the 6.7 GHz methanol maser range from 19.4 Jy (Yang et al. 2019) to 21.2 Jy (Szymczak et al. 2012), while those of the 12.2 GHz methanol maser vary from 4.7 Jy (Durjasz et al. 2021) to 8.2 Jy (this work), both peaking at approximately $-5.5$ km $s^{-1}$. Additionally, the velocity extent of the 6.7 GHz masers is between $-7$ and $-3$ km $s^{-1}$ (e.g., Yang et al. 2019), in contrast to the 12.2 GHz maser, which shows features between $-7$ and $-5$ km $s^{-1}$ in our observations.

*G85.410+0.003*. A strong 6.7 GHz methanol maser feature was detected in this source, with peak flux densities ranging from 42 Jy (Pestalozzi et al. 2005) to 140 Jy (Yonekura et al. 2016) at approximately $-30$ km $s^{-1}$. Its 12.2 GHz counterpart was first detected in 2017 January (Song et al. 2022) and again in 2019 August (Durjasz et al. 2021), displaying peak flux densities from about 3 Jy (Song et al. 2022) to 5.7 Jy (Durjasz et al. 2021), reaching 8 Jy in this study, all at approximately $-30$ km $s^{-1}$.

*G109.871+2.114*. Also known as Cepheus A (Cep A), this source is located in an HMSFR at a trigonometric distance of approximately 700 ± 40 pc (Moscadelli et al. 2009). It hosts an HMYSO with an estimated mass of approximately 10 $M_{\odot}$ and a bolometric luminosity of $2 \times 10^4$ $L_{\odot}$ (Sanna et al. 2017). Numerous observations of the associated 6.7 GHz methanol maser have documented a significant flare that persisted for about 1800 days. During this outburst, the peak flux density at 6.7 GHz varied markedly, ranging from approximately 1500 Jy (Menten 1991) to 400 Jy (Szymczak et al. 2012). In Durjasz et al. (2021), the peak flux density of the 12.2 GHz maser in this source was reported as 44.5 Jy, but in this work, it increased to 326 Jy, a factor of approximately 7.

*G111.542+0.777*. Also known as NGC 7538 and situated 2.65 kpc away (Moscadelli et al. 2009), this region is an HMSFR. It encompasses a prominent H II region, with star-forming complexes located along the western and southern peripheries. These complexes not only excite significant infrared sources but also potentially associate methanol masers with disks surrounding high-mass protostars (Pestalozzi et al. 2004). Observations indicate that the flux density of the 6.7 GHz methanol maser in this region ranges from approximately 150–300 Jy (Menten 1991; Surcis et al. 2012). The reported peak flux density of the 12.2 GHz methanol maser is 36.7 Jy (Durjasz et al. 2021), contrasting with the 67.3 Jy observed in this study.

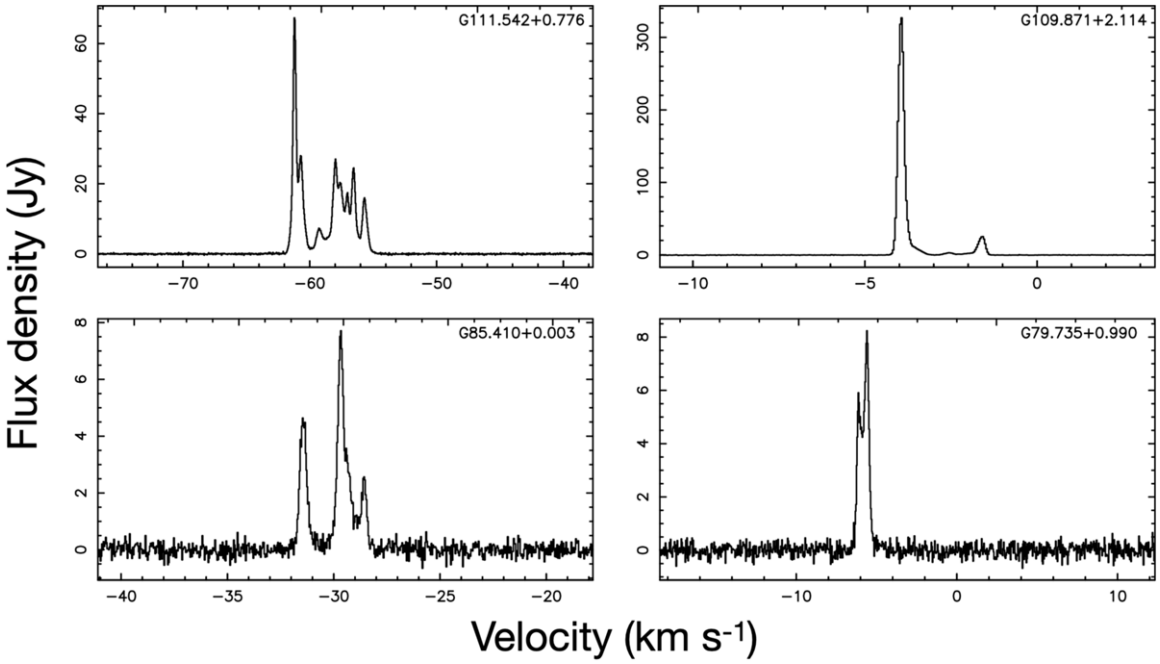


**Figure 1.** The spectra of the four 12.2 GHz methanol maser detections from the TMRT observations are presented. The source names are displayed in the upper right corners.

**Table 2**
The Characteristics of the Four Detected 12.2 GHz Methanol Masers

| Name (l, b) (1) | $V_{peak}$ (km s$^{-1}$) (2) | $\Delta V$ (km s$^{-1}$) (3) | $S_p$ (Jy) (4) | $I$ (Jy km s$^{-1}$) (5) | Epoch (Y–M–D) (6) |
|---|---|---|---|---|---|
| G79.736+0.991 | −5.60 | 0.57 | 8.20 | 6.04 | 20220718 |
| G85.410+0.003 | −29.66 | 2.11 | 7.70 | 8.13 | 20220718 |
| G109.871+2.114 | −3.93 | 1.54 | 326.80 | 102.00 | 20220718 |
| G111.542+0.777 | −61.21 | 4.75 | 67.30 | 105.00 | 20220718 |

**Note.** Column (1) lists the names of the sources. Columns (2) through (6) detail the peak velocity, velocity range, peak flux density, and integrated flux density. Column (6) records the date of the observations.

**Table 3**
The Characteristics of the All Detected 12.2 GHz Methanol Masers

| Name (l, b) (1) | R.A.(J2000.0) (hhmmss) (2) | Decl.(J2000.0) (ddmmss) (3) | $S_p$ (Jy) (4) | $V_{peak}$ (km s$^{-1}$) (5) | $\Delta V$ (km s$^{-1}$) (6) | $I$ (Jy km s$^{-1}$) (7) | References (8) |
|---|---|---|---|---|---|---|---|
| G0.212−0.001 | 17 46 07.63 | −28 45 20.9 | 0.8 | 49.4 | 48.9, 49.6 | 0.5 | MMB |
| G0.092−0.663 | 17 48 25.90 | −29 12 05.9 | 6.3 | 23.5 | 21.0, 23.9 | 3.9 | MMB |
| G0.315−0.201 | 17 47 09.13 | −28 46 15.7 | 2.4 | 18.2 | 17.7, 20 | 1.9 | MMB |
| G0.496+0.188 | 17 46 03.96 | −28 24 52.8 | 18.0 | 1.0 | −9.7, 1.5 | 16.0 | MMB |
| G0.546−0.852 | 17 50 14.53 | −28 54 31.2 | 3.9 | 18.4 | 13.7, 19.2 | 2.5 | MMB |
| G0.644−0.042 | 17 47 18.66 | −28 24 24.8 | 9.8 | 48.1 | 47.5, 55.7 | 5.8 | S22 |
| … | … | … | … | … | … | … | … |

**Note.** Column (1) lists the names of the 12.2 GHz methanol maser sources; an asterisk (*) indicates sources observed in this work. Columns (2) and (3) detail the coordinates of these sources. Columns (4) through (7) enumerate the peak flux density, peak velocity, velocity range, and integrated flux density, respectively. Column (8) cites the references for the sources: "MMB" refers to Breen et al. (2012a, 2012b, 2014, 2016), "D21" to Durjasz et al. (2021), and "S22" to Song et al. (2022). (The full table is available at https://www.scidb.cn/en/s/BjaUFz).

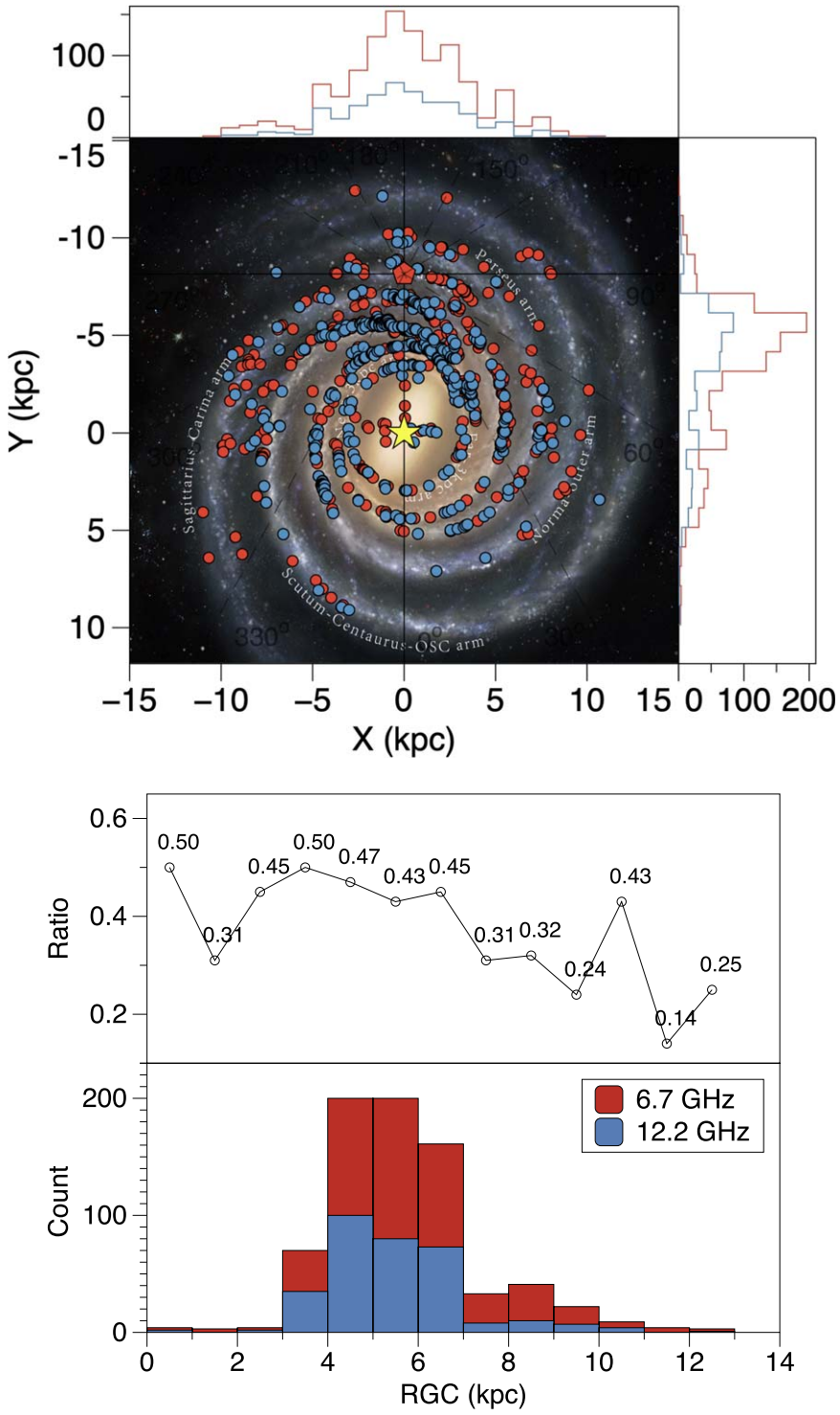


**Figure 2.** The spatial distribution of 6.7 and 12.2 GHz methanol masers within the Milky Way is shown. In the upper panel, red dots represent 6.7 GHz methanol masers, while blue dots indicate sources with both 6.7 and 12.2 GHz methanol masers. The Milky Way background image is credited to "Xing-Wu Zheng & Mark Reid, BeSSeL/NJU/CFA." The lower panel presents a histogram of the counts of 6.7 and 12.2 GHz methanol masers along the galactocentric distance, and the ratio of 12.2–6.7 GHz methanol masers.

**Table 4**
The Detection Rate of 12.2 GHz Methanol Maser toward 6.7 GHz Maser Sources of Different Arms in the Milky Way

| Type | Nor-Out | Per | Sag-Car | Scu-Cen | Loc |
|---|---|---|---|---|---|
| (1) | (2) | (3) | (4) | (5) | (6) |
| 6.7 GHz | 212 | 83 | 219 | 300 | 40 |
| 12.2 GHz | 107 | 37 | 85 | 129 | 7 |
| Ratio | 50.1% | 44.6% | 38.9% | 43.0% | 17.5% |

**Note.** Nor-Out represents the Norma–Outer arm, Per represents the Perseus arm, Sag-Car represents the Sagittarius–Carina arm, Scu-Cen represents the Scutum–Centaurus arm, and Loc is the Local arm.

**Table 5**
The Results of the Distance Calculator for Masers in Different Arms

| Name | Distance | Arm | 12.2? | Galactocentric azimuth |
|---|---|---|---|---|
| (l, b) | (kpc) | | Yes/No | (°) |
| (1) | (2) | (3) | (4) | (5) |
| G0.092-0.663 | 2.88 | Sc | Yes | 179.64 |
| G0.167-0.446 | 2.83 | Sc | No | 179.75 |
| G0.212-0.001 | 11.1 | 3kF | Yes | ⋯ |
| G0.315-0.201 | 2.86 | Sc | Yes | 179.80 |
| G0.316-0.201 | 2.87 | Sc | No | 179.80 |
| G0.376+0.040 | 6.76 | ... | No | ... |
| ⋯ | ⋯ | ⋯ | ⋯ | ⋯ |

**Note.** Column (1) is the names of sources. Column (2) lists the distances calculated through the BeSSeL project. Column (3) is the spiral arm of the source—Sc (Scutum far), Ct (Centaurus), N (Norma arm), N4N (Norma arm Q4 near), N4F (Norma arm Q4 far), Out (Outer arm), Per (Perseus arm), SgN (Sagittarius near), SgF (Sagittarius far), Cr (Carina), 3k (3 kpc arm), Loc (Local Arm), Los (local spur), AqS (Aquila spur), ... (unknown). Column (4) lists whether the source is associated with a 12.2 GHz methanol maser. Column (5) lists the Galactocentric azimuth of the source. For the Norma–Outer and Perseus arms, zero degree is set in the direction from the Galactic Center to the Sun, with positive angles measured counterclockwise. For the Scutum–Centaurus and Sagittarius–Carina arms, zero degree is set in the direction from the Sun to the Galactic Center, with positive angles also measured counterclockwise. (The full table is available at https://www.scidb.cn/en/s/BjaUFz).

## 4. Discussion

### *4.1. The 6.7 and 12.2 GHz Methanol Maser Overall Distributions*

Using the sample from Yang et al. (2019), which includes 1,085 known 6.7 GHz methanol masers, we determined that the overall detection rate of 12.2 GHz methanol masers in the Milky Way is approximately 42.2% (457/1085). This rate aligns with the results of the MMB survey, which reported a detection rate of 45.1% (438/972). Notably, nearly half of the 6.7 GHz methanol masers lack 12.2 GHz counterparts, a topic that will be discussed in Section 4.4. We analyze the distribution of 12.2 GHz methanol masers to identify differences between 12.2 and 6.7 GHz methanol masers within our galaxy. To improve the precision of locating these sources projected onto the arms, we set the weighting probability for the spiral arm at 0.85. This suggests that the distance calculator is not purely kinematic, but rather a combination of multiple approaches.

As depicted in the upper panel of Figure 2, it is clear that both 6.7 and 12.2 GHz methanol masers effectively trace the spiral arm structure of the Milky Way, providing substantial evidence of intense high-mass star formation activity along these arms. It is worth noting that this may be caused by weighting the spiral arms higher when calculating the distance. These masers are predominantly located near the Galactic center, but are rare within the 3 kpc ring. The apparent concentration of masers along the line-of-sight to the Galactic center may be attributable to an observational effect. In the lower panel of Figure 2, the density of both 6.7 and 12.2 GHz methanol masers peaks at a galactocentric distance of 5–6 kpc. This finding aligns with the distribution projected along the *Y*-axis in the upper panel of Figure 2. Given that these masers trace HMSFRs, it suggests that conditions at this distance are optimal for the high-mass stars formation. Additionally, the detection rates of the 12.2 GHz methanol masers across various galactocentric distances indicate that the highest rates occur within the 4–6 kpc range, supporting the idea that high-mass star formation is most likely concentrated within this region. This area also shows a higher propensity for the occurrence of 12.2 GHz methanol masers. This also might be a result of the higher spiral arms weighting of the distance calculation.

Song et al. (2022) argued that 12.2 GHz methanol masers are more commonly found in the relatively inner regions of the Milky Way, especially at the heads of the spiral arms, and are rare in the outer regions or the tails of the spiral arms. However, this observation was limited to data from the northern hemisphere. This conclusion is further supported when the results here are included. Regardless of their distance to the Sun, there is a higher detection rate of 12.2 GHz methanol masers closer to the Galactic center (see Figure 2). According to the pumping model presented in Cragg et al. (2005), 6.7 GHz methanol masers favor environments with lower temperatures and gas densities compared to 12.2 GHz methanol masers. This supports the notion of the inside-out Milky Way evolutionary scenario.

### *4.2. The 6.7 and 12.2 GHz Methanol Masers in Different Arms*

In this section, we analyze the 6.7 and 12.2 GHz methanol masers across the Milky Way's four major spiral arms (e.g., Shen & Zheng 2020). The detection rates of 12.2 GHz methanol masers associated with 6.7 GHz masers in these arms are as follows (see Table 4): 50.1% in the Norma–Outer arm, 44.6% in the Perseus arm, 38.9% in the Sagittarius–Carina arm, and 43.0% in the Scutum–Centaurus arm, generally

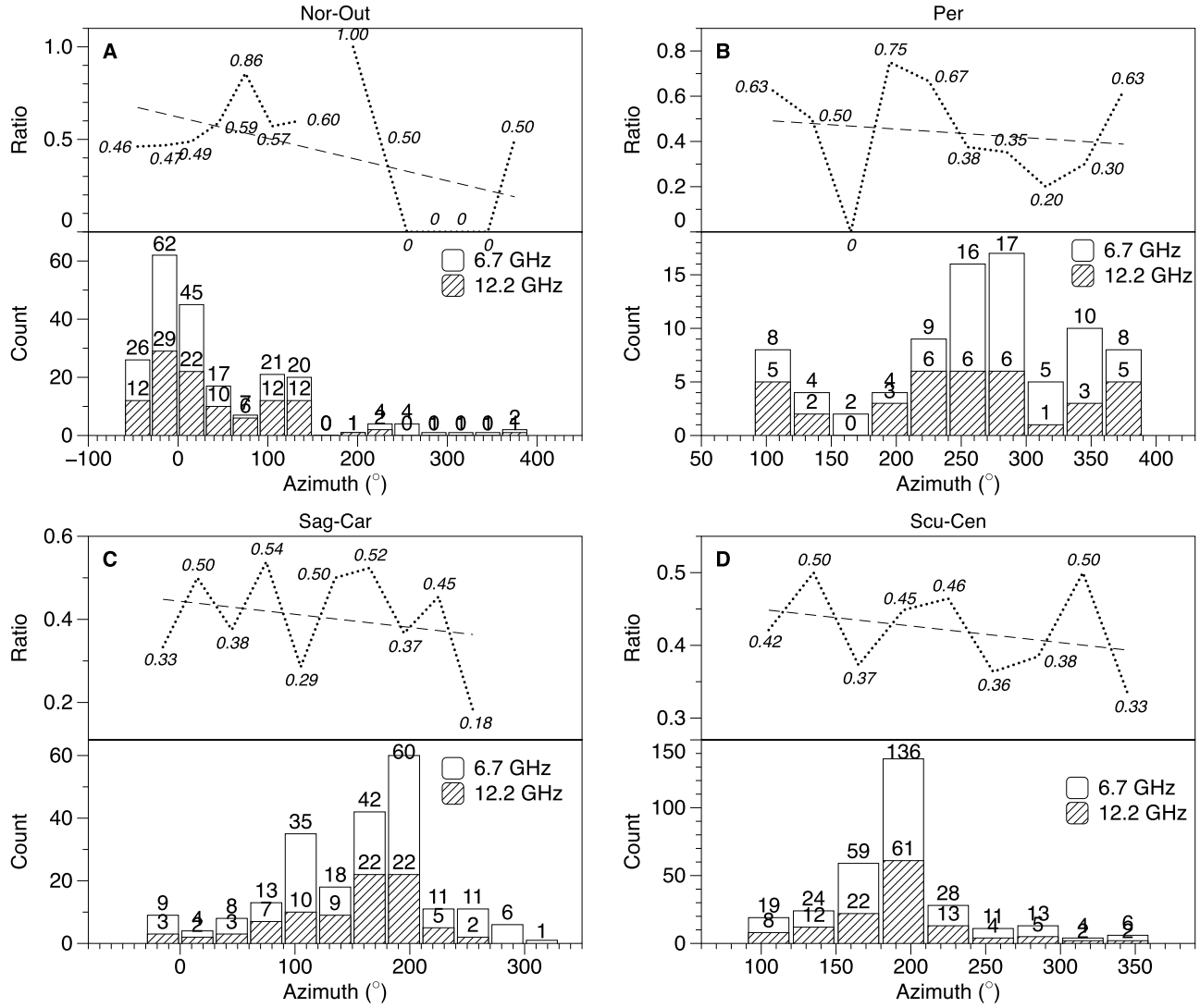


**Figure 3.** The detection rate of 12.2 GHz methanol masers in various spiral arms is shown as a function of their Galactocentric azimuth with a bin size of 30°. The title for each panel is the same as Table 4.

ranging from 40% to 50%. The detection rate of 12.2 GHz masers is about two times lower, at 17.5% (seven versus forty 6.7 GHz masers), toward the Local Arm. This may not be statistically significant, ergo we do not consider it further.

Notably, the detection rate of 38.9% in the Sagittarius–Carina arm is lower than in the other arms. This variance contrasts with Song et al. (2022), which reported an approximate 50% detection rate across the four arms. It is important to note that Song et al. (2022) focused on the northern hemisphere, closer to the Galactic center, analyzing regions associated with both 6.7 GHz methanol masers and H II regions, potentially influencing their higher reported detection rates.

We focus on the detection rate for individual spiral arms to further examine the hypothesis that the detection rate is higher at the leading edges of the arms (Song et al. 2022). We calculate the Galactocentric azimuth of each spiral arm to define the head or tail of the arm (see Table 5). Figure 3 illustrates the variation in detection rate with Galactocentric azimuth, with a bin size of 30°. The Galactocentric azimuth ranges for the four arms are 241.°75, 322.°2, 424.°77, and 267.°23 for the Scutum–Centaurus, Sagittarius–Carina, Norma–Outer, and Perseus arms, respectively. Only the Norma–Outer arm shows higher maser productivity at the head of the arm; the other arms are more productive in the tails. However, all four arms exhibit a decreasing trend in detection rates with increasing Galactocentric azimuth.

To determine whether there are differences in the physical environments of 6.7 and 12.2 GHz methanol maser sources in different spiral arms, we conduct a statistical analysis of the

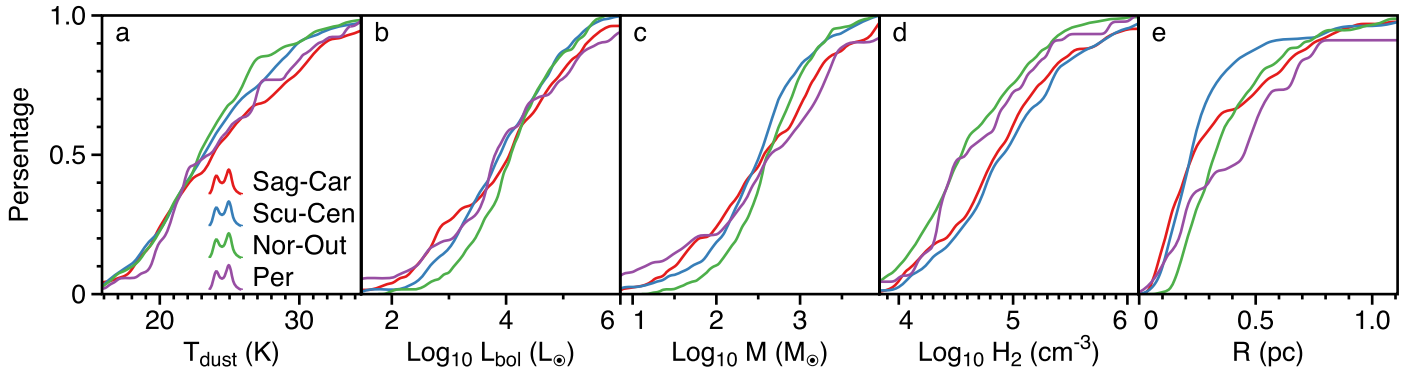


**Figure 4.** The cumulative distribution of various physical parameters of massive clumps across different spiral arms, based on the four-arm model of the Milky Way. Panels (a) to (e) respectively depict the distributions of dust temperature, bolometric luminosity, mass, hydrogen density, and radius. The Sagittarius–Carina arm is represented in red, the Scutum–Centaurus arm in blue, the Norma–Outer arm in green, and the Perseus arm in purple.

**Table 6**
The Parameter of ATLASGAL Survey of 783 Matched Sources

| Name (l, b) | $T_{dust}$ (K) | $R$ (pc) | $\log_{10} L$ ($L_\odot$) | $\log_{10} M$ ($M_\odot$) | $\log_{10} H_2$ ($cm^{-3}$) | EvoType |
|---|---|---|---|---|---|---|
| (1) | (2) | (3) | (4) | (5) | (6) | (7) |
| G3.253 +0.018 | 15.2 | 0.48 | 2.832 | 2.914 | 4.402 | PDR |
| G3.312-0.399 | 13.7 | 0.23 | 2.965 | 2.564 | 5.046 | YSO |
| G3.442-0.348 | 21.4 | 1.16 | 5.631 | 4.752 | 5.094 | H II region |
| G3.502-0.200 | 14.9 | 1.44 | 3.813 | 4.17 | 4.231 | Protostellar |
| G3.910 +0.001 | 29.7 | 0.08 | 3.567 | 1.543 | 5.32 | H II region |
| … | … | … | … | … | … | … |

**Note.** Column (1) provides the names of the sources, specified by Galactic longitude and latitude. Columns (2)–(7) display the dust temperature, clump radius, bolometric luminosity, clump mass, hydrogen density, and evolutionary type, respectively, as provided by the ATLASGAL survey. (The full table is available at https://www.scidb.cn/en/s/BjaUFz).

physical parameters of HMSFRs associated with these masers in the Milky Way. We cross-match our sample sources with the ATLASGAL survey (Urquhart et al. 2022) to extract physical parameters such as dust temperature and bolometric luminosity. The matching radius is set at 30″, aligning with the APEX telescope's beam size. Also, if the $V_{lsr}$ of the ATLASGAL clump is within 5 km s$^{-1}$ of the peak pulsation speed, it is considered a successful match. This process yields 783 matched sources, as detailed in Table 6.

We performed cumulative distribution analysis (see Figure 4) on various physical parameters and conducted Kolmogorov–Smirnov (K-S) tests between different spiral arms to distinguish the differences in the physical parameters of massive clumps across the four spiral arms (details in Table 7). Significant differences in dust temperature ($T_{dust}$) distributions were identified only between the Sagittarius–Carina and Norma–Outer spiral arms. As shown in Figure 4, the dust temperature in the Sagittarius–Carina arm is noticeably higher than in the Norma–Outer arm. Although some significant distribution differences were found between spiral arms for dust temperature ($T_{dust}$), bolometric luminosity ($L_{bol}$), and clump mass ($M$), the distribution lines of most spiral arms in Figure 4 are significantly blended, making it difficult to distinguish differences in these aspects. However, in terms of hydrogen density ($H_2$) and clump radius ($R$), most spiral arms exhibit distinct distribution differences. Notably, between the Sagittarius–Carina (lowest 12.2 GHz detection rate) and Norma–Outer (highest 12.2 GHz detection rate) arms, the Sagittarius–Carina arm has a higher hydrogen density but a smaller clump size. This aligns with the evolutionary pattern, where density and temperature rise as size contracts. The higher dust temperature and hydrogen density in the Sagittarius–Carina arm may thermally quench the 12.2 GHz maser emission.

### *4.3. The Luminosities of 6.7 and 12.2 GHz Methanol Masers*

The presence of a 12.2 GHz methanol maser typically indicates the existence of a 6.7 GHz counterpart. The close relationship between their luminosities has been observationally confirmed by many studies (e.g., Breen et al. 2011, 2016). In this section, we expand the sample to include 6.7 and 12.2 GHz masers throughout the entire Milky Way to further explore the luminosity relationship between these two types of methanol masers. We calculated the luminosities using distances determined by the BeSSeL project distance calculator (Reid et al. 2016; Reid et al. 2019), as introduced in Section 4.1.

**Table 7**
The K-S Test Results for the Four Different Galaxy Arms Regarding the ATLASGAL Survey Physical Parameters

| Parameter | Statistics | Sag-Car/Scu-Cen | Sag-Car/Nor-Out | Sag-Car/Per | Scu-Cen/Nor-Out | Scu-Cen/Per | Nor-Out/Per |
|---|---|---|---|---|---|---|---|
| $T_{dust}$ | *P*-value | 0.16 | 0.02 | 0.92 | 0.11 | 0.59 | 0.15 |
| | *D*-value | 0.12 | 0.17 | 0.09 | 0.12 | 0.12 | 0.18 |
| $L_{bol}$ | *P*-value | 0.20 | 5.53E-03 | 0.65 | 0.19 | 0.61 | 0.2 |
| | *D*-value | 0.11 | 0.19 | 0.11 | 0.15 | 0.11 | 0.06 |
| Mass | *P*-value | 5.83E-03 | 0.19 | 0.75 | 0.04 | 0.02 | 0.28 |
| | *D*-value | 0.18 | 0.58 | 0.11 | 0.74 | 0.23 | 0.54 |
| $H_2$ density | *P*-value | 0.67 | 9.80E-06 | 0.03 | 1.72E-08 | 3.93E-03 | 0.64 |
| | *D*-value | 0.08 | 0.29 | 0.24 | 0.31 | 0.28 | 0.12 |
| Radius | *P*-value | 7.79E-03 | 4.39E-06 | 0.08 | 1.89E-09 | 1.96E-05 | 0.41 |
| | *D*-value | 0.18 | 0.29 | 0.21 | 0.32 | 0.38 | 0.49 |

**Note.** The K-S test parameters, *D*-value—the maximum difference between the cumulative distributions of two compared samples; *P*-value— if the K-S test returns a *p*-value <0.05, the difference between the two compared samples is thought to be significant.

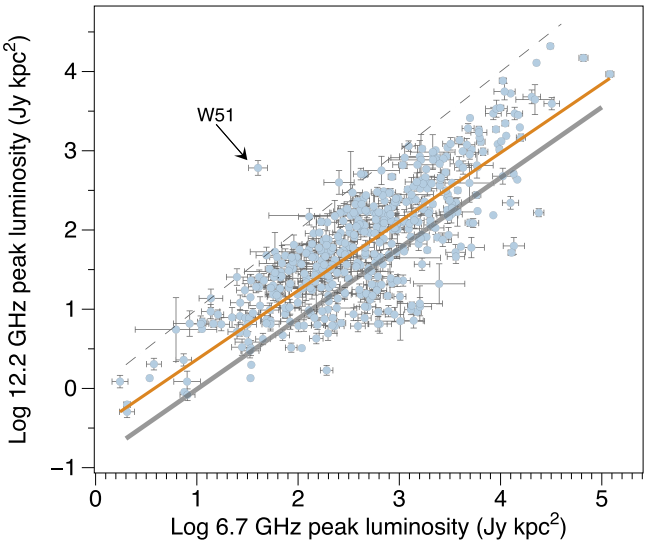


**Figure 5.** The flux correlation analysis between the 6.7 and 12.2 GHz methanol masers. The yellow line is the best fitting line. The gray dashed line has a slope of 1. The gray solid line represent the result from Breen et al. (2016). The errors are represented with bars.

### *4.3.1. The Relationship of 6.7 and 12.2 GHz Methanol Maser Luminosities*

Based on data from the MMB survey, Breen et al. (2016) conducted a correlation analysis on the luminosities of 6.7 and 12.2 GHz masers, finding a strong positive correlation with a fitted slope of 0.84 ± 0.03. Song et al. (2022) utilized the TMRT survey results to study the luminosity correlation between 6.7 and 12.2 GHz methanol masers across 176 sources, concluding that they are highly correlated with a fitted slope of 0.73 ± 0.05. In this work, we supplement the data by analyzing the correlation of the overall luminosities of 6.7 and 12.2 GHz methanol masers for a more comprehensive sample, including data from the MMB and TMRT surveys across the Milky Way. The most comprehensive luminosity fitting equation (goodness of fit $R^2 = 0.64$) for these two masers derived from the current analysis is (see Figure 5):

$$\log_{10}(L_{6.7}) = 0.87[0.02]\log_{10}(L_{12.2}) - 0.50[0.06] \quad (1)$$

where $L_{6.7}$ and $L_{12.2}$ are the luminosities of the 6.7 and 12.2 GHz methanol masers, respectively, in units of Jy kpc$^2$. The numbers in brackets are the errors for each fitting parameter.

In Figure 5, a notable outlier is observed within the data set. This outlier corresponds to the source G49.471−0.369, commonly known as W51. W51 is a well-known complex of HMSFRs and is likely experiencing an accretion outburst event (Meyer et al. 2017). The entire giant molecular cloud associated with this source has a mass exceeding $10^6$ $M_\odot$ and hosts stars at various stages of formation, including remnants of supernovae (Ginsburg et al. 2017). W51 is typically classified into three main sections: W51A, W51B, and W51C. The peak velocities of the 6.7 and 12.2 GHz methanol masers for this source do not align exactly, suggesting a significant difference in the spatial distribution of these masers at different frequencies. Zhang et al. (2022) identified multiple velocity components traced by ammonia and water in their study of W51 IRS2. The flux of the 6.7 GHz methanol maser ranges from approximately 3 Jy (Pandian et al. 2011) to 850 Jy (Malyshev & Sobolev 2003), while the 12.2 GHz methanol maser flux varies from about 2 Jy (Breen et al. 2016) to 20 Jy (Song et al. 2022). This deviation is likely attributed to differences in observation epochs, though further detailed investigations are necessary to elucidate the specific reasons.

Additionally, we conducted a statistical analysis of both 6.7 and 12.2 GHz maser luminosities (see Figure 6). Song et al. (2022)

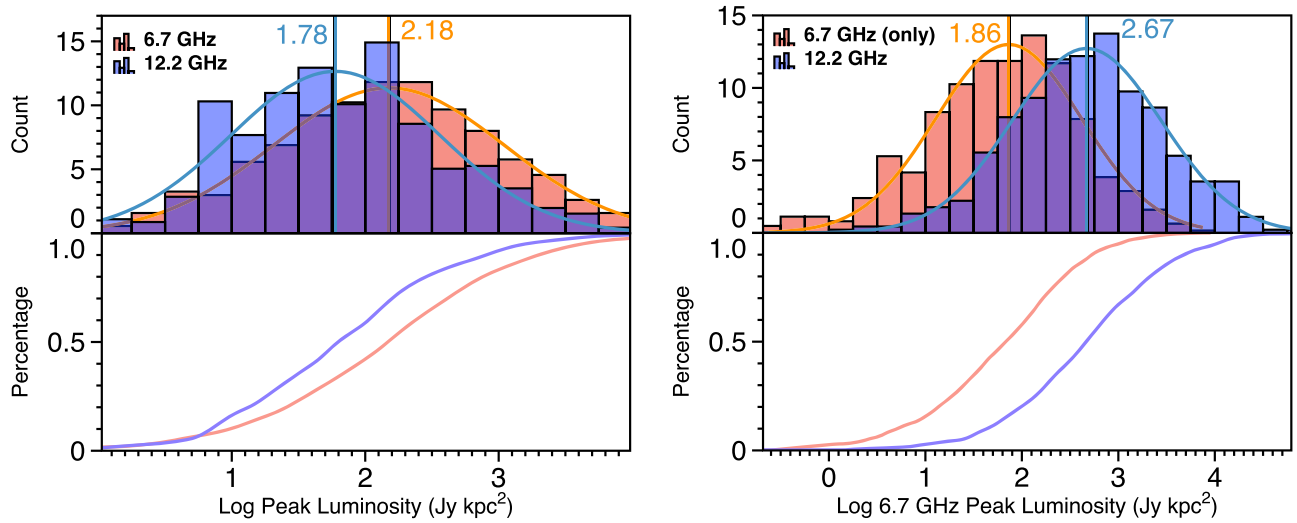


**Figure 6.** The luminosity distribution of 6.7 and 12.2 GHz methanol masers in the Milky Way is illustrated. The top left panel depicts the luminosity distribution of both the 6.7 and 12.2 GHz methanol masers, while the bottom left panel shows their cumulative distributions. In the top right panel, the quantity distribution of 6.7 GHz methanol maser luminosity is presented for sources with only the 6.7 GHz maser and for those with both the 6.7 and 12.2 GHz masers, with median values of 1.86 and 2.67, respectively. Their cumulative distributions are displayed in the bottom right panel.

examined the luminosity distribution relationship between 6.7 and 12.2 GHz methanol masers associated with H II regions. In this study, we expand upon their findings by enlarging the sample to include 6.7 and 12.2 GHz methanol masers across the entire Milky Way and applying a K-S test to the data, further supporting the earlier results. In the left panel of Figure 6, the luminosity distribution of both 6.7 and 12.2 GHz masers within the Milky Way closely aligns, consistent with the model proposed by Cragg et al. (2005). Although the intensity of the 6.7 GHz maser appears stronger than that of the 12.2 GHz maser, the result of the K-S test (p-value = 0.47) indicates that the 6.7 and 12.2 GHz methanol masers are statistically similar. In the right panel of Figure 6, it is evident that the luminosity of 6.7 GHz masers from sources with only 6.7 GHz masers is lower than that of sources with both 6.7 and 12.2 GHz masers. The K-S test shows a significant difference between the two distributions ($p$-value $= 3 \times 10^{-43}$). Generally, the more luminous 6.7 GHz methanol maser sources are associated with the later evolutionary stage of high-mass star formation (Breen et al. 2010), while sources with only 6.7 GHz methanol masers exhibit significantly lower peak luminosities compared to those with both 6.7 and 12.2 GHz methanol masers (see Figure 6). This further corroborates the scheme proposed by Breen et al. (2010), indicating that the 12.2 GHz methanol maser stage occurs later than that of the 6.7 GHz methanol maser.

### *4.3.2. The Relationship between the Physical Parameters and Maser Luminosity*

Dust temperature and gas density significantly influence the excitation intensity of 6.7 and 12.2 GHz methanol masers (Cragg et al. 2005). Using data from the ATLASGAL survey (Urquhart et al. 2022), we conducted a statistical analysis to examine the relationship between the physical parameters of massive clumps-such as dust temperature, bolometric luminosity, and hydrogen density, and the luminosity of 6.7 and 12.2 GHz methanol masers (detailed in Figure 7). This analysis aims to explore the distribution differences of 6.7 and 12.2 GHz methanol masers across various physical parameter spaces. Although the goodness of fit for all parameters is less than 0.6, these fits are used solely to demonstrate trend changes.

The upper two panels of Figure 7 depict the statistical analysis of the luminosity of 12.2 and 6.7 GHz methanol masers concerning clump physical parameters such as dust temperature, hydrogen density, and bolometric luminosity. The maser luminosities exhibit varying degrees of increase with these parameters. Specifically, 6.7 GHz maser luminosities peak at approximately 30 K of dust temperatures, while the 12.2 GHz maser luminosities continue to increase with temperature. This indicates that the intensity of 6.7 GHz masers rises and then diminishes as the temperature increases, whereas the 12.2 GHz maser luminosity continues to grow. These findings imply that warmer sources are less conducive to the excitation of 6.7 GHz masers but more conducive to 12.2 GHz masers. The lower panels of Figure 7 compare the luminosity ratios of the two masers with various physical parameters. Both the 6.7 and 12.2 GHz masers' luminosities, as well as the 6.7/12.2 luminosity ratio, increase with rising hydrogen density and bolometric luminosity. While higher hydrogen densities and bolometric luminosities positively influence the excitation of both masers, the 6.7 GHz maser grows faster than the 12.2 GHz maser as the densities and luminosities increase.

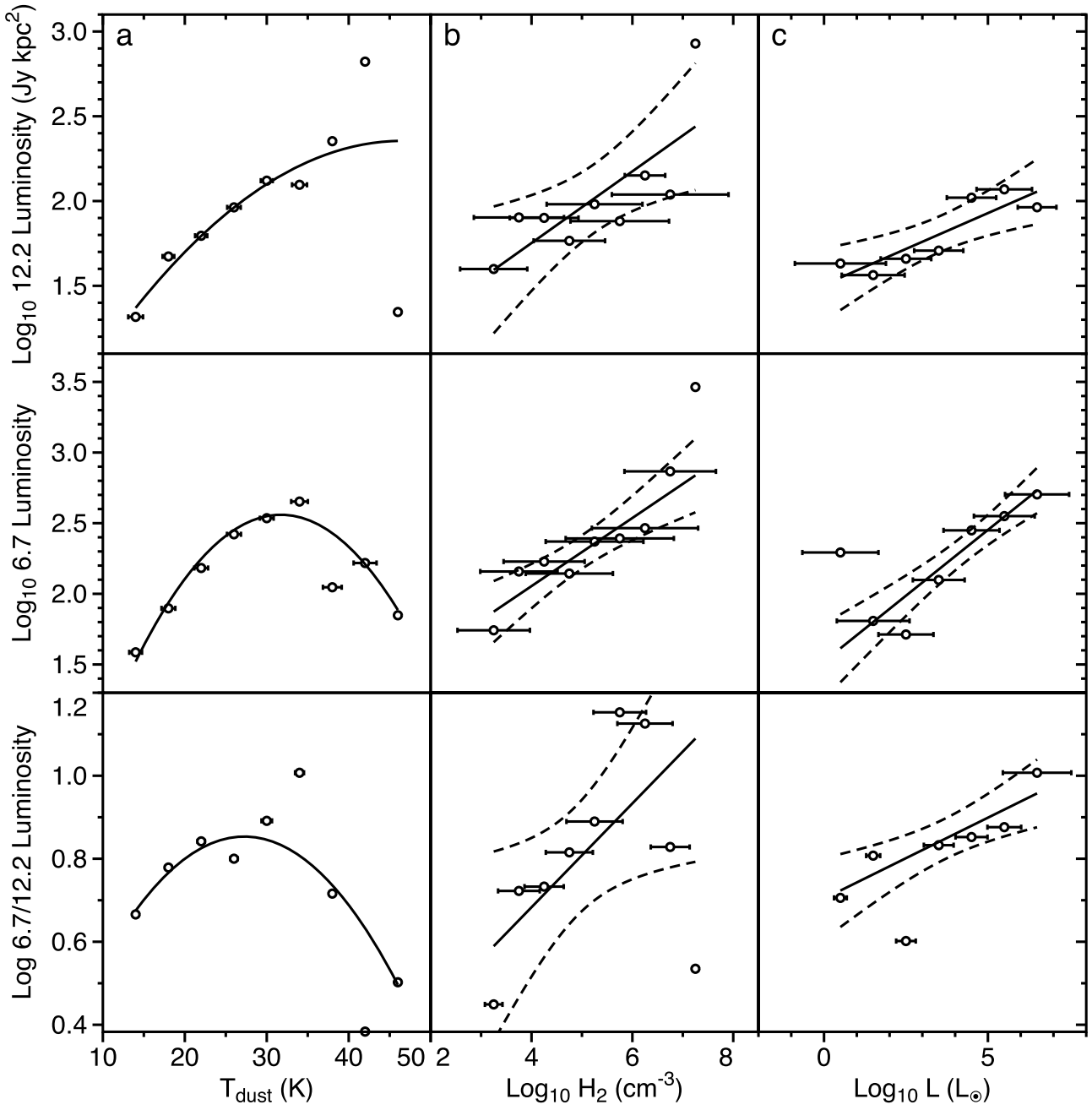


**Figure 7.** The correlation between the luminosities of 6.7, 12.2 GHz methanol masers and the physical parameters of their host clumps. The upper two and lower panels depict, respectively, the relationship between the peak luminosity of 6.7, 12.2 GHz masers, the ratio of peak luminosities at 6.7 and 12.2 GHz, and the parameters of their host clumps. Panels (a) through (c) specifically represent dust temperature, hydrogen density, and bolometric luminosity, respectively. The solid line in each panel represents the fit to the data, and the dashed lines denote the 95% confidence intervals.

### *4.4. The Evolutionary Stages of 6.7 and 12.2 GHz Methanol Masers*

As previously mentioned, over half of the sources exhibit only the 6.7 GHz methanol maser, without detection of the 12.2 GHz counterpart (e.g., Breen et al. 2012a, 2016; Durjasz et al. 2021; Song et al. 2022). Theoretically, the excitation conditions for both types of methanol masers are similar, yet there are subtle differences (Sobolev & Deguchi 1994; Sobolev et al. 1997). The physical conditions required to excite 12.2 GHz masers are more stringent than those for 6.7 GHz

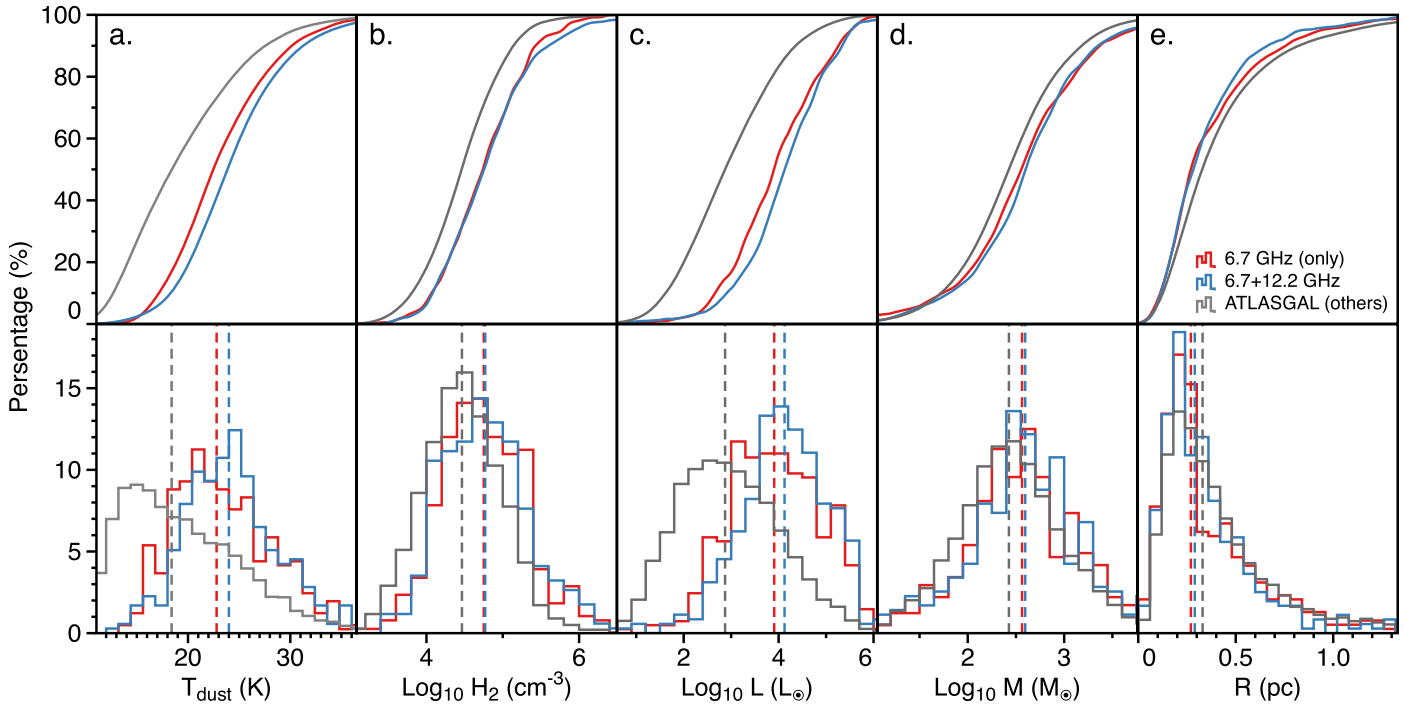


**Figure 8.** The distribution disparities among the 6.7 GHz methanol masers, the 12.2 GHz methanol masers, and the distribution of the ATLASGAL massive clumps without masers. The upper panels are the cumulative distribution, and the lower panels are histograms. Panels (a) to (e) respectively represent dust temperature, hydrogen density, bolometric luminosity, mass, and radius. The red lines indicate the sources associated with 6.7 GHz methanol masers only, the blue lines represent the sources associated with both 6.7 and 12.2 GHz methanol masers, and the gray lines represent the rest of the ATLASGAL survey, which are sources associated with neither 6.7 nor 12.2 GHz methanol maser. The dashed lines signify the median of the physical parameters for each group.

masers. Extreme temperatures or densities can result in the disappearance of the 12.2 GHz masers, while the 6.7 GHz masers are likely to persist (Sobolev et al. 1997). Research by Breen et al. (2010) indicates that the luminosity of the 6.7 GHz maser intensifies as its host source evolves. In the right panel of Figure 6, there are indications of evolutionary differences between the 6.7 and 12.2 GHz masers. Sources with only the 6.7 GHz maser are less luminous than those with a counterpart 12.2 GHz maser, suggesting that sources associated with 12.2 GHz masers are more evolved. To test this hypothesis, we conducted a cumulative distribution analysis using data from ATLASGAL (see Figure 8).

Through the statistical analysis of the physical parameters of sources with only 6.7 GHz methanol masers, both 6.7 and 12.2 GHz methanol masers, and other ATLASGAL massive clumps (Figure 8), we found distinct differences in bolometric luminosity and dust temperature among the three groups. The K-S test results are listed in Table 8. The median bolometric luminosities for high-mass star-forming clumps associated with only 6.7 GHz masers, both 6.7 and 12.2 GHz masers, and other ATLASGAL massive clumps are $10^{3.9}$, $10^{4.1}$, and $10^{2.9}$ $L_{\odot}$, respectively. The median dust temperatures are 22.8, 24.0, and 18.2 K, respectively. While no significant differences are

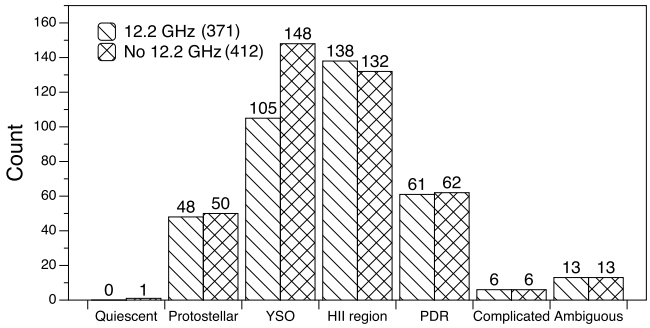


**Figure 9.** The statistics of the sources with and without 12.2 GHz methanol maser in different evolutionary types. The evolutionary types are extracted from the ATLASGAL survey (Urquhart et al. 2022).

observed in other physical parameters between the distributions of the 6.7 and 12.2 GHz masers, notable differences exist between sources with and without masers. Sources with masers generally have higher hydrogen densities and clump masses but smaller clump sizes. This suggests that the high-mass star formation stages traced by masers are relatively late, characterized by higher temperature, luminosity, and gas density but smaller size in massive clumps. For sources with

**Table 8**
The K-S Test Results for the Three Groups Regarding the ATLASGAL Survey Physical Parameters

| Parameter | Statistics | 6.7/6.7+12.2 | 6.7/others | Others/6.7+12.2 |
|---|---|---|---|---|
| $T_{dust}$ | *P*-value | 9.67E−03 | 3.91E−47 | 5.39E−62 |
| | *D*-value | 0.12 | 0.37 | 0.45 |
| $H_2$ density | *P*-value | 0.86 | 4.48E−13 | 3.97E−13 |
| | *D*-value | 0.04 | 0.20 | 0.21 |
| $L_{bol}$ | *P*-value | 2.36E−03 | 2.75E−54 | 6.84E−75 |
| | *D*-value | 0.13 | 0.39 | 0.49 |
| Mass | *P*-value | 0.24 | 2.68E−05 | 9.60E−10 |
| | *D*-value | 0.07 | 0.12 | 0.18 |
| Radius | *P*-value | 0.67 | 1.35E−03 | 0.02 |
| | *D*-value | 0.05 | 0.10 | 0.08 |

**Note.** The K-S test parameters, *D*-value—the maximum difference between the cumulative distributions of two compared samples; *P*-value— if the K-S test returns a *p*-value <0.05, the difference between the two compared samples is thought to be significant.

masers, those with 12.2 GHz masers also have relatively higher temperatures and luminosities, implying that the evolutionary stage of 12.2 GHz maser sources is more advanced than that of 6.7 GHz maser sources.

Based on the evolutionary stage classification of ATLASGAL (Urquhart et al. 2022), we conducted statistical analysis on the masers associated with sources at different evolutionary stages (see Figure 9). Most of the 6.7 and 12.2 GHz methanol masers are located in the YSO and H II region stages, with the 12.2 GHz maser detection rates being 42% (105/253) and 51% (138/270), respectively. The 12.2 GHz masers are more likely to be excited at the H II region stage, while sources only associated with 6.7 GHz masers are more commonly in the YSO stage. This further supports the idea that 12.2 GHz masers may occur in later stages than 6.7 GHz masers, consistent with our earlier discussion.

## 5. Summary

Building on previous work, we compiled a comprehensive catalog of 12.2 GHz methanol maser sources in the Milky Way, incorporating data from the TMRT, MMB, and other surveys. By integrating results from the BeSSeL project and the ATLASGAL survey, we conducted a statistical analysis of the large-scale spatial distribution, luminosity correlation, physical parameters of associated clumps, and evolutionary sequences of the 6.7 and 12.2 GHz methanol masers in the Milky Way. The main findings of this paper are summarized as follows:

1. *Catalog*. By combining observations from the MMB survey (Breen et al. 2012a, 2012b, 2014, 2016; Song et al. 2022; Durjasz et al. 2021), we identified 457 12.2 GHz methanol masers in the Milky Way. Using the catalog of 1085 6.7 GHz methanol maser sources provided by Yang et al. (2019), we determined that the detection rate of 12.2 GHz methanol masers is 42% among the 6.7 GHz methanol masers.
2. *Distributions*. Masers are more likely excited around galactocentric distances of 5–6 kpc. The detection rate of 12.2 GHz methanol masers increases with proximity to the Galactic center, indicating more active high-mass star formation near the center. The detection rate in the Sagittarius–Carina arm is comparatively low, possibly due to higher temperature and density gas clumps in this arm, as indicated by ATLASGAL sources. Additionally, comprehensive data confirm a higher detection rate of 12.2 GHz methanol masers at the heads of the spiral arms compared to the tails.
3. *Correlation and Evolution*. Using a more comprehensive sample, we further reveal the positive correlation between the luminosities of 6.7 and 12.2 GHz methanol masers. Additionally, sources that contain both 6.7 and 12.2 GHz masers generally exhibit higher 6.7 GHz methanol maser luminosities compared to those containing only 6.7 GHz masers. By analyzing the physical parameters obtained from the ATLASGAL survey, we find that massive clumps associated with 12.2 GHz masers have significantly higher dust temperatures and bolometric luminosities than those with only 6.7 GHz masers. This further indicates that the evolutionary stage of 12.2 GHz methanol masers is generally later than that of 6.7 GHz masers.

## Acknowledgments

This work is supported by the National Key R&D Program of China (2022YFA1603102), the National Natural Science Foundation of China (11873002, 12011530065, and 11590781), and China Postdoctoral Science Foundation (2023M740803). X.C. thanks the Guangdong Province Universities and Colleges Pearl River Scholar Funded Scheme (2019). This work is also supported by the Great Bay Center and, National Astronomical Data Center. Y.X.W. is a member of the International Max Planck Research School (IMPRS) for Astronomy and Astrophysics at the Universities of Bonn and Cologne.

## Data Availability

The TMRT data used in this article will be shared on reasonable request to the corresponding author. The ATLASGAL data is available in the publication by Uchiyama et al. (2022). The MMB data is available in the publications: Breen et al. (2012a, 2012b, 2014, 2016).

## ORCID iDs

Shi-Min Song https://orcid.org/0000-0003-3640-3875

## References


Batrla, W., Matthews, H. E., Menten, K. M., & Walmsley, C. M. 1987, Natur, 326, 49
Błaszkiewicz, L., & Kus, A. J. 2004, A&A, 413, 233
Breen, S. L., Ellingsen, S. P., Caswell, J. L., & Lewis, B. E. 2010, MNRAS, 401, 2219
Breen, S. L., Ellingsen, S. P., Caswell, J. L., et al. 2011, ApJ, 733, 80
Breen, S. L., Ellingsen, S. P., Caswell, J. L., et al. 2012a, MNRAS, 421, 1703
Breen, S. L., Ellingsen, S. P., Caswell, J. L., et al. 2012b, MNRAS, 426, 2189
Breen, S. L., Ellingsen, S. P., Contreras, Y., et al. 2013, MNRAS, 435, 524
Breen, S. L., Ellingsen, S. P., Caswell, J. L., et al. 2016, MNRAS, 459, 4066
Breen, S. L., Ellisngsen, J. L., Caswell, J. A., et al. 2014, MNRAS, 438, 3368
Breen, S. L., Fuller, G. A., Caswell, J. A., et al. 2015, MNRAS, 450, 4109
Breen, S. L., Contreras, Y., Ellingsen, S. P., et al. 2018, MNRAS, 474, 3898
Bussa, S. & VEGAS Development Team 2012, AAS Meeting Abstracts, 219, 446.10
Caratti o Garatti, A., Stecklum, B., Garcia Lopez, R., et al. 2017, NatPh, 13, 276
Caswell, J. L., Vaile, R. A., Ellingsen, S. P., & Norris, R. P. 1995, MNRAS, 274, 1126
Caswell, J. L., Fuller, G. A., Green, J. A., et al. 2010, MNRAS, 404, 1029
Caswell, J. L., Fuller, G. A., Green, J. A., et al. 2011, MNRAS, 417, 1964
Chen, X., Ellingsen, S. P., Gan, C., Xu, Y., & Shen, Z. 2014, ChSBu, 59, 1066
Chen, X., Ellingsen, S. P., Ren, Z.-Y., et al. 2019, ApJ, 877, 90
Chen, X., Sobolev, A. M., Ren, Z. Y., et al. 2020, NatAs, 4, 1170
Cragg, D. M., Sobolev, A. M., & Godfrey, P. D. 2005, MNRAS, 360, 533
Durjasz, M., Szymczak, M., Wolak, P., & Bartkiewicz, A. 2021, A&A, 648, A118
Ellingsen, S. P. 2006, ApJ, 638, 241
Ginsburg, A., Goddi, C., Diederik Kruijssen, J. M., et al. 2017, ApJ, 842, 92
Goedhart, S., Minier, V., Gaylard, M. J., & van der Walt, D. J. 2005, MNRAS, 356, 839
Green, J. A., Caswell, J. L., Fuller, G. A., et al. 2009, MNRAS, 392, 783
Green, J. A., Caswell, J. L., Fuller, G. A., et al. 2010, MNRAS, 409, 913
Green, J. A., Caswell, J. L., Fuller, G. A., et al. 2012, MNRAS, 420, 3108
Green, J. A., Breen, S. L., Fuller, G. A., et al. 2017, MNRAS, 469, 1383
Hunter, T. R., Brogan, C. L., MacLeod, G. C., et al. 2017, ApJL, 837, L29
Hunter, T. R., Brogan, C. L., MacLeod, G. C., et al. 2018, ApJ, 854, 170
Kobak, A., Bartkiewicz, A., Szymczak, M., et al. 2023, A&A, 671, A135
Liu, S.-Y., Su, Y.-N., Zinchenko, I., Wang, K.-S., & Wang, Y. 2018, ApJL, 863, L12
MacLeod, G. C., Gaylard, M. J., & Nicolson, G. D. 1992, MNRAS, 254, 1P
MacLeod, G. C., Scalise, E. J., Saedt, S., Galt, J. A., & Gaylard, M. J. 1998, AJ, 116, 1897
Malyshev, A. V., & Sobolev, A. M. 2003, A&AT, 22, 1
Menten, K. M. 1991, ApJL, 380, L75
Menten, K. M., & Melnick, G. J. 1991, ApJ, 377, 647
Meyer, D. M. A., Vorobyov, E. I., Kuiper, R., & Kley, W. 2017, MNRAS, 464, L90
Moscadelli, L., Reid, M. J., Menten, K. M., et al. 2009, ApJ, 693, 406
Pandian, J. D., Momjian, E., Xu, Y., Menten, K. M., & Goldsmith, P. F. 2011, ApJ, 730, 55
Pestalozzi, M. R., Elitzur, M., Conway, J. E., & Booth, R. S. 2004, ApJL, 603, L113
Pestalozzi, M. R., Minier, V., & Booth, R. S. 2005, A&A, 432, 737
Reid, M. J., Dame, T. M., Menten, K. M., & Brunthaler, A. 2016, ApJ, 823, 77
Reid, M. J., Menten, K. M., Brunthaler, A., et al. 2019, ApJ, 885, 131
Sanna, A., Moscadelli, L., Surcis, G., et al. 2017, A&A, 603, A94
Shen, J., & Zheng, X.-W. 2020, RAA, 20, 159
Sobolev, A. M., Cragg, D. M., & Godfrey, P. D. 1997, A&A, 324, 211
Sobolev, A. M., & Deguchi, S. 1994, A&A, 291, 569
Song, S.-M., Chen, X., Shen, Z.-Q., et al. 2022, ApJS, 258, 19
Surcis, G., Vlemmings, W. H. T., van Langevelde, H. J., & Hutawarakorn Kramer, B. 2012, A&A, 541, A47
Szymczak, M., Wolak, P., Bartkiewicz, A., & Borkowski, K. M. 2012, AN, 333, 634
Uchiyama, M., Ichikawa, K., Sugiyama, K., Tanabe, Y., & Yonekura, Y. 2022, ApJ, 936, 31
Urquhart, J. S., König, C., Giannetti, A., et al. 2018, MNRAS, 473, 1059
Urquhart, J. S., Wells, M. R. A., et al. 2022, MNRAS, 510, 3389
van der Walt, D. J., Gaylard, M. J., & MacLeod, G. C. 1995, A&AS, 110, 81
Yang, K., Chen, X., Shen, Z.-Q., et al. 2017, ApJ, 846, 160
Yang, K., Chen, X., Shen, Z.-Q., et al. 2019, ApJS, 241, 18
Yonekura, Y., Saito, Y., Sugiyama, K., et al. 2016, PASJ, 68, 74
Zhang, Y.-K., Chen, X., Sobolev, A. M., et al. 2022, ApJS, 260, 34